

PXR OF A DIVERGING ELECTRON BEAM IN A MAGNETIZED SINGLE CRYSTAL

A. NOSKOV

Moscow Technical University of Communications and Informatics, st. Aviamotornaya, 8a., Moscow, 111024, Russia.

E-mail: noskovbupk@mail.ru

Received

Abstract. A dynamic theory of coherent X-ray radiation of beams of relativistic electrons intersecting a single-crystal plate is developed, taking into account magnetic permeability. Expressions describing the spectral-angular and angular densities of parametric X-ray radiation are obtained and investigated, taking into account the divergence of the beam of relativistic electrons and the magnetic permeability of the single crystal.

Key words: parametric x-ray, magnetized single crystal, relativistic electron beam.

1. INTRODUCTION

If a charged particle crosses a single crystal, its Coulomb field is scattered by a system of parallel atomic planes of the single crystal, generating parametric X-ray radiation (PXR) near the Bragg scattering direction [1–3]. There are kinematic [4,5] and dynamic [2,3] approaches to describing the PXR generation process. Unlike the dynamic approach, the kinematic approach takes into account the interaction of each atom only with the primary wave in the single crystal, i.e., it neglects the interaction of the atom with the wave field created in the single crystal by the combined scattering by all other atoms. Within the framework of the two-wave approximation of the dynamic theory of diffraction, coherent X-ray radiation of relativistic electrons in a single crystal plate was considered in [6–7], where the joint contribution of PXR and diffracted transition radiation was taken into account. In the Bragg scattering geometry, parametric X-ray radiation of a relativistic electron is considered in detail in the monograph [8], which describes many works carried out over a fairly long period of time. Further development of the dynamic theory of PXR and DTR of a relativistic electron in a single crystal was presented in the works [9-11] for the general case of asymmetric reflection of the electron field relative to the target surface, when the system of parallel reflecting layers of the target can be located at any given angle to the target surface. It is also necessary to note the great interest in recent years in the generation of

PXR of relativistic electrons in periodic layered media in a wide X-ray range [12-17].

In all the cited works, coherent X-ray radiation in single crystals and periodic layered media was considered without taking into account the magnetic properties of the medium, i.e. when the magnetic permeability of the medium is equal to unity $\mu = 1$. It is known that the magnetic permeability of natural tungsten is not initially equal to unity, its value is $\mu_w = 1,000068$, and its permittivity at the radiation frequency $\omega = 8keV$ takes the values $\epsilon_w = 0,99990441$.

The real parts of the dielectric and magnetic susceptibility at this radiation frequency take the values: $\chi'_\mu = 6,8 \cdot 10^{-5}$ and $\chi'_\epsilon = -9,5 \cdot 10^{-5}$. They have the same order of smallness, and with an increase in the radiation frequency, the value of χ'_ϵ will decrease in absolute value and the magnetic susceptibility can have an increasingly significant effect on the PXR. In [18], a theory of coherent X-ray radiation of a relativistic electron in a magnetized single-crystal plate was constructed. An expression was obtained and investigated that describes the spectral-angular density of the PXR, containing the magnetic permeability of the single crystal.

In a real experiment, beams of relativistic electrons with a certain initial angular divergence are used. The angular divergence of the electron beam can have a significant effect on the spectral-angular and angular densities of PXR. Since the peak width of the PXR spectrum in a single crystal is usually on the order of 1-2 eV, the angular density of PXR is a common measured value in the experiment. The angular divergence of a beam of relativistic electrons can greatly affect the angular density of radiation. This work is devoted to the study of the influence of the magnetic permeability of the medium on the spectral-angular and angular densities of PXR. In this work, a theory of PXR of a beam of relativistic electrons is developed. It is shown that within the framework of the two-wave approximation of the dynamic diffraction theory, two branches of X-ray waves with different dependences of the length of the photon wave vector on the radiation frequency can make a significant contribution to the angular density of PXR for a certain magnetic permeability of the medium, depending on specific conditions. Expressions describing the spectral-angular and angular densities of two branches of PXR are obtained and investigated, taking into account the magnetic properties of a single-crystal plate and the angular divergence of a beam of relativistic electrons.

2. DYNAMIC X-RAY DIFFRACTION IN A MAGNETIZED SINGLE CRYSTAL

Let us consider the radiation of a relativistic electron in a single crystal (Fig.1). The notations introduced by Fig.1: θ is radiation angle relative to detector axis \mathbf{e}_2 ; θ_0 is the angle of photon propagation \mathbf{n} relative to beam axis \mathbf{e}_1 ; ψ is incidence angle of an electron with velocity \mathbf{V} relative to beam axis \mathbf{e}_1 ; θ is radiation angle relative to detector axis \mathbf{e}_2 ; \mathbf{n}_g is the direction of propagation of a scattered photon near the Bragg scattering direction; ψ_0 is the angular divergence of the electron beam; δ is the angle of inclination of planes of a single crystal relative to the target surface.

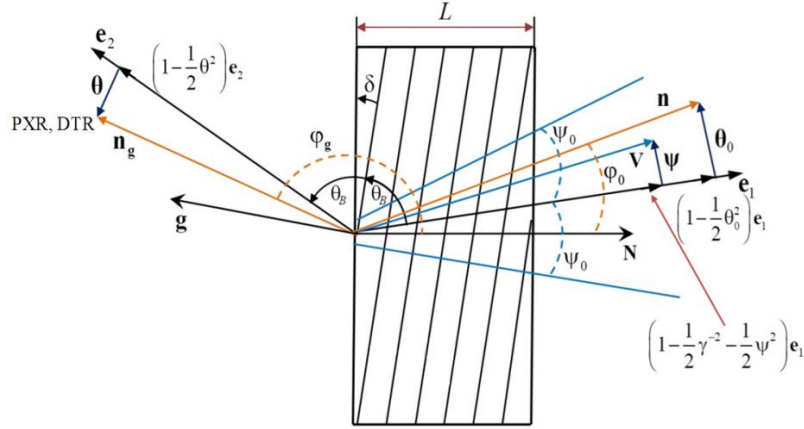


Fig. 1 – Geometry of radiation in a multilayer structure

The vectors under consideration can be represented as:

$$\begin{aligned} \boldsymbol{\theta}_0 &= \boldsymbol{\theta}_{0\parallel} + \boldsymbol{\theta}_{0\perp}, \quad \boldsymbol{\theta} = \boldsymbol{\theta}_{\parallel} + \boldsymbol{\theta}_{\perp}, \quad \boldsymbol{\psi} = \boldsymbol{\psi}_{\parallel} + \boldsymbol{\psi}_{\perp}, \\ \mathbf{V} &= \left(1 - \frac{1}{2}\gamma^{-2} - \frac{1}{2}\psi^2\right)\mathbf{e}_1 + \boldsymbol{\psi}, \quad \mathbf{n}_g = \left(1 - \frac{1}{2}\theta^2\right)\mathbf{e}_2 + \boldsymbol{\theta}, \quad \mathbf{n} = \left(1 - \frac{1}{2}\theta_0^2\right)\mathbf{e}_1 + \boldsymbol{\theta}_0, \\ \mathbf{e}_1\boldsymbol{\psi} &= 0, \quad \mathbf{e}_1\boldsymbol{\theta}_0 = 0, \quad \mathbf{e}_1\mathbf{e}_2 = \cos 2\theta_B, \quad \mathbf{e}_2\boldsymbol{\theta} = 0. \end{aligned} \quad (1)$$

$\gamma = 1/\sqrt{1-V^2}$ - Lorentz factor of the electron; \mathbf{g} - reciprocal lattice vector. The modulus of the reciprocal lattice vector g is determined by the expression $g = 2\omega_B \sin\theta_B / V$, where ω_B is the Bragg frequency, θ_B is Bragg angle. The wave vectors of the incident and diffracted photons have the form: $\mathbf{k} = \omega\mathbf{n}$, $\mathbf{k}_g = \omega\mathbf{n}_g$. Vectors $\boldsymbol{\theta}_{\perp}$, $\boldsymbol{\theta}_{0\perp}$ and $\boldsymbol{\psi}_{\perp}$ are perpendicular to the plane of vectors \mathbf{k} and \mathbf{k}_g . Vectors $\boldsymbol{\theta}_{\parallel}$, $\boldsymbol{\theta}_{0\parallel}$ and $\boldsymbol{\psi}_{\parallel}$ are parallel to the plane of vectors \mathbf{k} and \mathbf{k}_g .

Considering the field strength vector of a relativistic particle to be transverse, we expand the strengths of the incident and diffracted waves into unit polarization vectors:

$$\mathbf{E}_{\omega, \mathbf{k}} = E_{\omega, \mathbf{k}}^{(1)} \mathbf{e}^{(1)} + E_{\omega, \mathbf{k}}^{(2)} \mathbf{e}^{(2)}, \quad \mathbf{E}_{\omega, \mathbf{k} + \mathbf{g}} = E_{\omega, \mathbf{k} + \mathbf{g}}^{(1)} \mathbf{e}_g^{(1)} + E_{\omega, \mathbf{k} + \mathbf{g}}^{(2)} \mathbf{e}_g^{(2)}. \quad (2)$$

Let us write the polarization vectors we have chosen as follows:

$$\mathbf{e}^{(1)} = \mathbf{e}_g^{(1)} = \frac{[\mathbf{k}, \mathbf{g}]}{[\mathbf{k}, \mathbf{g}]}, \quad \mathbf{e}^{(2)} = \frac{[\mathbf{k}, \mathbf{e}^{(1)}]}{k}, \quad \mathbf{e}_g^{(2)} = \frac{[\mathbf{k}_g, \mathbf{e}^{(1)}]}{k_g}. \quad (3)$$

In expansions (2), the polarization vectors $\mathbf{e}^{(1)}$ and $\mathbf{e}^{(2)}$ are perpendicular to the vector \mathbf{k} , and the vectors $\mathbf{e}_g^{(1)}$ and $\mathbf{e}_g^{(2)}$ are perpendicular to the vector $\mathbf{k} + \mathbf{g}$. Further, we will use the notation $\mathbf{k}_g = \mathbf{k} + \mathbf{g}$. The vectors $\mathbf{e}^{(2)}$ and $\mathbf{e}_g^{(2)}$ lie in the plane formed by the vectors \mathbf{k} and \mathbf{k}_g , we will call the corresponding field strengths π -polarized. The vectors $\mathbf{e}^{(1)}$ and $\mathbf{e}_g^{(1)}$ are perpendicular to the plane of the vectors \mathbf{k} and \mathbf{k}_g (σ -polarization).

From the usual system of Maxwell equations for the electromagnetic field, an expression for the Fourier images is obtained, describing the relationship between the intensities of the incident field $\mathbf{E}_{\omega, \mathbf{k}}$, and the diffracted field $\mathbf{E}_{\omega, \mathbf{k} + \mathbf{g}}$ in a single crystal, as well as the current density $\mathbf{j}_{\omega, \mathbf{k}}$:

$$\left(k^2 - \mu\omega^2(1 + \chi_0(\omega))\right)\mathbf{E}_{\omega, \mathbf{k}} - \mathbf{k}(\mathbf{k}\mathbf{E}_{\omega, \mathbf{k}}) - \mu\omega^2 \sum_{\mathbf{g} \neq 0} \chi_{-\mathbf{g}}(\omega)\mathbf{E}_{\omega, \mathbf{k} + \mathbf{g}} = 4\pi i\omega\mu\mathbf{j}_{\omega, \mathbf{k}}. \quad (4)$$

Where μ is the magnetic permeability of the single crystal, ω is the frequency of X-ray radiation, $\chi_0(\omega)$ is the average dielectric susceptibility in the single crystal, $\chi_{\mathbf{g}}(\omega) = \chi'_{\mathbf{g}}(\omega) + i\chi''_{\mathbf{g}}(\omega)$ is the expansion coefficient of the dielectric susceptibility in terms of the reciprocal lattice vectors:

$$\chi(\omega) = \chi_0(\omega) + \sum_{\mathbf{g} \neq 0} \chi_{\mathbf{g}}(\omega) e^{i\mathbf{g}\mathbf{r}}.$$

It should be noted that the real part of the expansion of the dielectric susceptibility in terms of the reciprocal lattice vectors of the $\chi'_{\mathbf{g}}$ is determined by the expression:

$$\chi'_{\mathbf{g}} = \chi'_0(F(\mathbf{g})/Z)(S(\mathbf{g})/N_0) \exp\left(-\frac{1}{2}g^2 u_{\tau}^2\right),$$

where $F(\mathbf{g})$ is the form factor of an atom containing Z electrons, $S(\mathbf{g})$ is the structural factor of the unit cell containing N_0 atoms, u_τ is the root-mean-square amplitude of thermal vibrations of the crystal atoms. The work considers the X-ray frequency range ($\chi'_g < 0, \chi'_0 < 0$). The imaginary part of $\chi_g(\omega)$ is determined by the expression:

$$\chi''_g = \chi''_0 \exp\left(-\frac{1}{2} g^2 u_\tau^2\right).$$

The imaginary and real parts of the average dielectric susceptibility are determined by the expressions:

$$\chi'_0 = -\frac{1}{Z} f_1 \frac{\omega_0^2}{\omega^2}, \quad \chi''_0 = \frac{1}{Z} f_2 \frac{\omega_0^2}{\omega^2},$$

where, $\omega_0 = \sqrt{\frac{4\pi n e^2}{m}}$ is the plasma frequency of oscillation of electrons of the medium, n is the density of electrons of the medium, e is the charge of the electron, m is the mass of the electron. The quantities f_1 and f_2 are the real and imaginary parts, respectively, of the atomic scattering function $f = f_1 + if_2$, which depends on the atom of the substance and the frequency of the radiation. In calculations, the values of these quantities are usually taken from tables.

Let us consider the two-wave approximation of the dynamic theory of diffraction. Two strong waves are formed in a single crystal, the rest are negligibly small, which corresponds to the reflection of X-ray waves from one system of parallel atomic planes of the single crystal. The incident and diffracted waves transform into each other and constructively interfere. The wave vectors of these waves \mathbf{k} and \mathbf{k}_g , differ by the reciprocal lattice vector of the considered system of parallel atomic planes of the single crystal \mathbf{g} . Let us substitute expressions (2) into (4) and carry out the corresponding transformations within the framework of the two-wave approximation of the dynamic theory of diffraction. We obtain a system of equations for the Fourier transforms of the amplitudes of the electric field strengths of the incident and diffracted waves, which contains the magnetic permeability μ :

$$\begin{aligned} \left(k^2 - \mu\omega^2(1 + \chi_0(\omega))\right) E_{\omega, \mathbf{k}}^{(s)} - \mu\omega^2 \chi_{-\mathbf{g}}(\omega) E_{\omega, \mathbf{k}+\mathbf{g}}^{(s)} C^{(s, \tau)} &= 8\pi^2 i \mu \omega e \Omega^{(s)} \delta(\omega - \mathbf{kV}), \\ \left((\mathbf{k} + \mathbf{g})^2 - \mu\omega^2(1 + \chi_0(\omega))\right) E_{\omega, \mathbf{k}+\mathbf{g}}^{(s)} - \mu\omega^2 \chi_{\mathbf{g}}(\omega) E_{\omega, \mathbf{k}}^{(s)} C^{(s, \tau)} &= 0, \end{aligned} \quad (5)$$

where the following notations are introduced:

$$\begin{aligned} C^{(s,\tau)} &= \mathbf{e}_{\mathbf{g}}^{(s)} \mathbf{e}^{(s)} = (-1)^\tau C^{(s)}, \quad C^{(1)} = 1, \quad C^{(2)} = |\cos 2\theta_B|, \\ \Omega^{(1)} &= \mathbf{e}_0^{(1)} \mathbf{V} = \theta_\perp - \psi_\perp, \quad \Omega^{(2)} = \mathbf{e}_0^{(2)} \mathbf{V} = \theta_\parallel + \psi_\parallel. \end{aligned} \quad (6)$$

The system of equations (5) for $s=1$ and $\tau=2$ describes σ -polarized fields. For $s=2$, the system of equations describes π -polarized fields, and if $2\theta_B < \frac{\pi}{2}$, then $\tau=2$, otherwise $\tau=1$.

From the system of equations (5) follows the dispersion relation:

$$(k_{\mathbf{g}}^2 - \mu\omega^2(1 + \chi_0))(k^2 - \mu\omega^2(1 + \chi_0)) - \mu^2\omega^4\chi_{-\mathbf{g}}\chi_{\mathbf{g}}C^{(s,\tau)^2} = 0. \quad (7)$$

Let us find the solution to equation (7) in the form:

$$k = \omega\sqrt{\mu(1 + \chi_0)} + \lambda_0, \quad k_{\mathbf{g}} = \omega\sqrt{\mu(1 + \chi_0)} + \lambda_{\mathbf{g}}. \quad (8)$$

Let's use the expression that connects the dynamic additives λ_0 and $\lambda_{\mathbf{g}}$:

$$\lambda_{\mathbf{g}} = \frac{\omega\beta}{2} + \lambda_0 \frac{\gamma_{\mathbf{g}}}{\gamma_0}. \quad \text{Where: } \beta = \frac{1}{\omega^2}(k_{\mathbf{g}}^2 - k^2) - \mu\chi_0 \left(1 - \frac{\gamma_{\mathbf{g}}}{\gamma_0}\right), \quad \gamma_{\mathbf{g}} = \cos\varphi_{\mathbf{g}}, \quad \gamma_0 = \cos\varphi_0.$$

φ_0 is the angle between \mathbf{k} and the normal vector \mathbf{N} , $\varphi_{\mathbf{g}}$ is the angle between $\mathbf{k}_{\mathbf{g}}$ and \mathbf{N} .

Substituting (8) into (7), we take into account the small value of the dynamic additives: $|\lambda_0| \ll \omega$ and $|\lambda_{\mathbf{g}}| \ll \omega$. We obtain expressions for the lengths of the wave vectors of X-ray radiation in a thin non-absorbing target, near the velocity of the relativistic electron $k_{(1,2)}^{(s)}$ and near the direction of Bragg scattering $k_{\mathbf{g}(1,2)}^{(s)}$:

$$k_{(1,2)}^{(s)} = \omega\sqrt{\mu(1 + \chi_0)} + \frac{\omega|\chi'_{\mathbf{g}}|C^{(s)}}{2\varepsilon} \left(\xi^{(s)}(\omega) \mp \sqrt{\xi^{(s)}(\omega)^2 - \varepsilon\mu} \right), \quad (9)$$

$$k_{\mathbf{g}(1,2)}^{(s)} = \omega\sqrt{\mu(1 + \chi_0)} + \frac{\omega|\chi'_{\mathbf{g}}|C^{(s)}}{2} \left(\xi^{(s)}(\omega) \pm \sqrt{\xi^{(s)}(\omega)^2 - \varepsilon\mu} \right), \quad (10)$$

where $\varepsilon = |\gamma_{\mathbf{g}}|/\gamma_0$ is the asymmetry parameter, $\xi^{(s)}(\omega)$ is the frequency function (12). We see that photons with wave vector lengths $k_{\mathbf{g}(1)}^{(s)}$ and $k_{\mathbf{g}(2)}^{(s)}$ can contribute to the PXR, that is, under certain conditions, two branches of PXR can exist and contribute to the radiation.

3. ANGULAR DENSITIES OF TWO BRANCHES PXR

We will solve the system of equations (5) for the electric fields inside the single-crystal plate, as well as outside it, under the conditions: $\chi_{-g} = \chi_0 = 0$ and $\mu = 1$. Applying the usual boundary conditions on the input and output surfaces of the target, we obtain an expression for the amplitude of the Fourier transform of the electric field strength of the PXR photons. Then, using the well-known expression for the spectral-angular density of radiation:

$$\omega \frac{d^3 N}{d\omega d\theta_{\perp} d\theta_{\parallel}} = \omega^2 (2\pi)^{-6} \sum_{s=1}^2 |E_{PXR}^{(s)}|^2,$$

we obtain expressions describing the spectral-angular densities of two branches of the PXR of a relativistic electron crossing a non-absorbing ($\chi_0'' = 0$) thin monocrystalline plate with magnetic permeability μ :

$$\omega \frac{d^3 N_{PXR(1,2)}^{(s)}}{d\omega d\theta_{\perp} d\theta_{\parallel}} = \frac{e^2 \varepsilon^2}{\pi^2 \mu^2} \frac{\Omega^{(s)2}}{\left(\Gamma - \chi_0' - 2(1 - 1/\sqrt{\mu})\right)^2} \frac{\Sigma_{(1,2)}^{(s)}}{F^{(s)}(\eta^{(s)})} \frac{\sin^2 \left(\frac{b^{(s)} \Sigma_{(1,2)}^{(s)}}{2} \right)}{\left(\Sigma_{(1,2)}^{(s)}\right)^2}. \quad (11)$$

In formula (11) the following notations are introduced:

$$\begin{aligned} \Gamma &= \gamma^{-2} + (\theta_{\perp} - \psi_{\perp})^2 + (\theta_{\parallel} + \psi_{\parallel})^2, \\ \Delta_1^{(s)} &= (\Delta_1'^{(s)} + 2\mu^2 \sigma_*^{(s)})^2 - 8\mu^2 \sigma_*^{(s)} \Delta_1'^{(s)} \sin^2 \left(\frac{b^{(s)} \Delta_2'^{(s)}}{2} \right), \\ \Delta_2^{(s)} &= (\Delta_2'^{(s)} + 2\mu^2 \sigma_*^{(s)})^2 - 8\mu^2 \sigma_*^{(s)} \Delta_2'^{(s)} \sin^2 \left(\frac{b^{(s)} \Delta_1'^{(s)}}{2} \right), \\ \Sigma_{(1,2)}^{(s)} &= \frac{\xi^{(s)} \mp \sqrt{\xi^{(s)2} - \varepsilon\mu}}{\varepsilon} - \sqrt{\mu} \sigma_*^{(s)}, \\ F^{(s)}(\eta^{(s)}) &= \xi^{(s)2} - \varepsilon\mu + \varepsilon\mu \sin^2 \left(\frac{b^{(s)} \sqrt{\xi^{(s)2} - \varepsilon\mu}}{\varepsilon} \right), \\ \sigma_*^{(s)} &= \sigma^{(s)} - \frac{2}{|\chi_g'| C^{(s)}} \left(1 - \frac{1}{\sqrt{\mu}} \right), \quad \sigma^{(s)} = \omega L_{ext}^{(s)} \left((\theta_{\perp} - \psi_{\perp})^2 + (\theta_{\parallel} + \psi_{\parallel})^2 + \gamma^{-2} - \chi_0' \right), \\ \xi^{(s)}(\omega) &= \eta^{(s)}(\omega) + \frac{\mu(1 + \varepsilon)}{2\nu^{(s)}}, \quad \eta^{(s)}(\omega) = \frac{2 \sin^2 \theta_B}{V^2 |\chi_g'| C^{(s)}} \left(1 - \frac{\omega(1 - \theta_{\parallel} \operatorname{ctg} \theta_B)}{\omega_B} \right), \end{aligned}$$

$$b^{(s)} = \frac{1}{2 \sin(\theta_B + \delta)} \frac{L}{L_{ext}^{(s)}}, L_{ext}^{(s)} = \frac{1}{\omega |\chi'_g| C^{(s)}}, \varepsilon = \frac{\sin(\theta_B - \delta)}{\sin(\theta_B + \delta)}, C^{(1)} = 1, C^{(2)} = |\cos 2\theta_B|. \quad (12)$$

For $s=1$, expressions (11) и (12) describe the fields σ - polarized, and for $s=2$ the fields π - polarized.

$\eta^{(s)}(\omega)$ is a rapidly changing function with a change in the radiation frequency in the vicinity of the Bragg frequency ω_B , since the inequality $\frac{2 \sin^2 \theta_B}{V^2 |\chi'_g| C^{(s)}} \gg 1$ is satisfied. $b^{(s)}$ is a parameter equal to the ratio of half the path

length of an electron in a plate $L_e = \frac{L}{\sin(\theta_B + \delta)}$ to the extinction length of X-ray

radiation in a single crystal $L_{ext}^{(s)}$.

The parameter ε determines the asymmetry of the electron field reflection relative to the target surface. Fig. 1 shows the arrangement of the reflecting atomic planes, at which the angle between the surface and the atomic planes is positive $\delta > 0$, in this case: $\varepsilon < 1$. In the case of symmetric reflection: $\delta = 0$ and $\varepsilon = 1$. In the case of a decrease in the angle between the electron velocity and the target surface, at a fixed θ_B , the angle δ becomes negative: $\delta < 0$ and $\varepsilon > 1$.

The contribution of the first and second branches to the spectral-angular density of the PXR will be significant when the denominator in the spectral part of expressions (11) is close to zero:

$$\Sigma^{(1)(s)} = \frac{\xi^{(s)} - \sqrt{\xi^{(s)2} - \varepsilon \mu}}{\varepsilon} - \sqrt{\mu \sigma_*^{(s)}} \approx 0, \quad (13)$$

$$\Sigma^{(2)(s)} = \frac{\xi^{(s)} + \sqrt{\xi^{(s)2} - \varepsilon \mu}}{\varepsilon} - \sqrt{\mu \sigma_*^{(s)}} \approx 0. \quad (14)$$

The solution of equations (13) and (14) determines the frequency ω^* , in the vicinity of which the spectrum of PXR photons emitted at a fixed angle $\theta(\theta_\perp, \theta_\parallel)$ is concentrated:

$$\xi^{(s)*}(\omega^*) = \sqrt{\varepsilon \mu} + \sqrt{\mu} \frac{(\sigma_*^{(s)} \sqrt{\varepsilon} - 1)^2}{2\sigma_*^{(s)}}, \quad (15)$$

where: $\sigma_*^{(s)} = \sigma^{(s)} - \frac{2}{|\chi'_g| C^{(s)}} \left(1 - \frac{1}{\sqrt{\mu}}\right)$, $\sigma^{(s)} = \frac{1}{|\chi'_g| C^{(s)}} \left((\theta_\perp - \psi_\perp)^2 + (\theta_\parallel + \psi_\parallel)^2 + \gamma^{-2} + |\chi'_0| \right)$.

It should be noted that the solution (15) is the same for the first and second branches of the PXR. However, the work revealed that the first branch of the PXR exists when the inequality is satisfied: $\sigma_*^{(s)} < \frac{1}{\sqrt{\varepsilon}}$, and the second exists when the inequality is satisfied: $\sigma_*^{(s)} > \frac{1}{\sqrt{\varepsilon}}$. It follows that in the case when the conditions: $\varepsilon \geq 1$ and $\mu = 1$ are satisfied, the inequality: $\sigma_*^{(s)} < \frac{1}{\sqrt{\varepsilon}}$ is not feasible, since the inequalities: $\sigma^{(s)} > 1$ and $\sigma_*^{(s)} > 1$ are always satisfied. In this case, the first branch of the PXR is not generated. But if the magnetic permeability is greater than unity $\mu > 1$, then the inequality $\sigma_*^{(s)} < \frac{1}{\sqrt{\varepsilon}}$ can be satisfied in the symmetric case ($\varepsilon = 1$) and even in the case of $\varepsilon > 1$ at certain values of the magnetic permeability μ , the Lorentz factor of the electron γ and the observation angle $\theta(\theta_{\perp}, \theta_{\parallel})$. In this case, the first branch of the PXR can be of significant importance. Thus, by increasing the magnetic permeability of a single crystal, it is possible to create conditions for a significant contribution of the first branch of the PXR, when the value of the asymmetry parameter is greater than or equal to one $\varepsilon \geq 1$. The second branch of the PXR can exist together with the first branch of the PXR at magnetic permeability values greater than one $\mu > 1$, but at different observation angles. Because at some observation angles the inequality $\sigma_*^{(s)} < \frac{1}{\sqrt{\varepsilon}}$ can be fulfilled, and at other observation angles the inequality: $\sigma_*^{(s)} > \frac{1}{\sqrt{\varepsilon}}$.

From solution (15) it follows that the maximum of the spectral density is in the region: $\xi^{(s)}(\omega) > \sqrt{\varepsilon\mu}$. The lengths of the wave vectors of two propagating X-ray waves in a magnetized single crystal have the form (9). From the moduli of the wave vectors (9) it follows that in the region of radiation frequencies corresponding to the inequality: $\xi^{(s)2} < \varepsilon\mu$, expressions (9) take complex values even in the absence of photoabsorption. Interference absorption of X-ray radiation occurs, which corresponds to maximum reflection. This region is called the frequency region of total external reflection of X-ray waves; in a magnetized single crystal it corresponds to the inequality:

$$-\sqrt{\varepsilon\mu} - \frac{\mu(1+\varepsilon)}{2\nu^{(s)}} < \eta^{(s)}(\omega) < \sqrt{\varepsilon\mu} - \frac{\mu(1+\varepsilon)}{2\nu^{(s)}}. \quad (16)$$

The width of this region is determined by the relation: $\Delta\eta^{(s)} = 2\sqrt{\varepsilon\mu}$.

From solution (15) and inequality (16) it follows that the frequency of the maximum of the PXR spectrum, as well as the width and location of the frequency region of total external reflection, depend on the magnetic permeability μ and the asymmetry parameter ε .

We obtain expressions describing the angular densities of the PXR. To do this, we integrate expressions (11) over the frequency function $\eta^{(s)}(\omega)$, using the relation: $\frac{d\omega}{\omega} = -\frac{|\chi'_g| C^{(s)}}{2 \sin^2 \theta_B} d\eta^{(s)}(\omega)$. The angular densities of the two branches of the PXR take the form:

$$\frac{d^2 N_{PXR(1,2)}^{(s)}}{d\theta_{\perp} d\theta_{\parallel}} = \frac{e^2 |\chi'_g| C^{(s)} \varepsilon^2}{\pi^2 2 \sin^2 \theta_B \mu^2} \frac{\Omega^{(s)2}}{\left(\Gamma - \chi'_0 - 2(1 - 1/\sqrt{\mu})\right)^2} \int_{\sqrt{\varepsilon\mu} - \frac{\mu(1+\varepsilon)}{2\nu^{(s)}}}^{\infty} \frac{\Sigma_{(1,2)}^{(s)}}{F^{(s)}(\eta^{(s)})} \times \frac{\sin^2\left(\frac{b^{(s)}\Sigma_{(1,2)}^{(s)}}{2}\right)}{\left(\Sigma_{(1,2)}^{(s)}\right)^2} d\eta^{(s)}, \quad (17)$$

Expressions (11) and (17) describe the spectral-angular and angular densities of the PXR taking into account the magnetic permeability of the single crystal μ . They are obtained for an electron moving at an angle $\psi(\psi_{\perp}, \psi_{\parallel})$ to the axis of the electron beam \mathbf{e}_1 . To take into account all possible rectilinear trajectories of electrons in the beam, it is necessary to average these expressions over the Gaussian distribution function:

$$f(\psi) = \frac{1}{\pi \psi_0^2} \exp\left(-\frac{\psi_{\perp}^2 + \psi_{\parallel}^2}{\psi_0^2}\right), \quad (18)$$

since in real beams the electrons are usually distributed at angles relative to the beam axis according to this distribution. The parameter ψ_0 will be called the divergence of the beam of emitting electrons (see Fig. 1).

We average expressions (11) and (17) over the electron distribution function in the beam (18). We obtain expressions describing the spectral-angular and angular densities of PXR, normalized to one electron, taking into account the angular divergence of the electron beam:

$$\left\langle \omega \frac{d^3 N_{PXR(1,2)}^{(s)}}{d\omega d\theta_{\perp} d\theta_{\parallel}} \right\rangle = \frac{e^2 \varepsilon^2}{\pi^3 \mu^2 \psi_0^2} \frac{1}{F^{(s)}(\eta^{(s)})} \times \int_{-\infty}^{+\infty} \int_{-\infty}^{+\infty} \frac{\Sigma_{(1,2)}^{(s)} \Omega^{(s)2} \exp\left(-\frac{\psi_{\perp}^2 + \psi_{\parallel}^2}{\psi_0^2}\right) \sin^2\left(\frac{b^{(s)}\Sigma_{(1,2)}^{(s)}}{2}\right)}{\left(\Gamma - \chi'_0 - 2(1 - 1/\sqrt{\mu})\right)^2 \left(\Sigma_{(1,2)}^{(s)}\right)^2} d\psi_{\perp} d\psi_{\parallel}, \quad (19)$$

$$\left\langle \frac{d^2 N_{PXR(1,2)}^{(s)}}{d\theta_{\perp} d\theta_{\parallel}} \right\rangle = \frac{e^2 |\chi'_g| C^{(s)} \varepsilon^2}{\pi^3 2 \sin^2 \theta_B \mu^2 \psi_0^2} \times$$

$$\times \int_{-\infty}^{\infty} \int_{-\infty}^{\infty} \frac{\Omega^{(s)2} \exp\left(-\frac{\psi_{\perp}^2 + \psi_{\parallel}^2}{\psi_0^2}\right)}{\left(\Gamma - \chi'_0 - 2(1 - 1/\sqrt{\mu})\right)^2} \left[\int_{\sqrt{\varepsilon\mu} - \frac{\mu(1+\varepsilon)}{2\nu^{(s)}}}^{\infty} \frac{\Sigma_{(1,2)}^{(s)} \sin^2\left(\frac{b^{(s)} \Sigma_{(1,2)}^{(s)}}{2}\right)}{F^{(s)}(\eta^{(s)}) \left(\Sigma_{(1,2)}^{(s)}\right)^2} d\eta^{(s)} \right] d\psi_{\perp} d\psi_{\parallel}. \quad (20)$$

The obtained expressions for the spectral-angular and angular densities of the PXR, taking into account the angular divergence of the electron beam, the asymmetry of the reflection of the electron field relative to the target surface and the magnetic permeability of the single crystal, are the main result of this work.

4. NUMERICAL CALCULATIONS AND ANALYSIS

Using the obtained expressions, we will perform numerical calculations for a specific case. Let us consider the radiation of a relativistic electron with the Lorentz factor $\gamma=500$, intersecting a single-crystal tungsten plate W(110) of thickness $L=10\mu\text{m}$. The angle between the axis of the electron beam \mathbf{e}_1 and the system of reflecting atomic planes of the single crystal (110) is equal to $\theta_B = 20,5^\circ$, in this case the Bragg frequency near which the radiation spectrum is formed is equal to $\omega_B = 8\kappa\varepsilon B$. At the radiation frequency under consideration, the real part of the average dielectric susceptibility of the tungsten single crystal has the value: $\chi'_0 = -9.6 \cdot 10^{-5}$. In this paper, we will restrict ourselves to the case of symmetric reflection, when the system of parallel atomic planes of the single crystal is parallel to the target surface ($\delta=0$ and $\varepsilon=1$). In the captions to some figures, the values for the natural magnetic permeability of the tungsten single crystal $\mu_w = 1.000068$ will be highlighted. The remaining values of magnetic permeability can be obtained by placing a single-crystal plate in a certain external magnetic field. The calculation will be carried out for σ -polarization, when $s=1$.

Fig. 2 shows the curves constructed using formula (11) describing the spectral-angular densities of the second branch of the PXR of a relativistic electron moving along the electron beam axis \mathbf{e}_1 , when $\psi_{\perp} = \psi_{\parallel} = 0$. The curves are constructed at a fixed observation angle: $\theta(\theta_{\perp}, \theta_{\parallel})$, where $\theta_{\perp} = 10\text{mrad}$, $\theta_{\parallel} = 0$. This angle corresponds to the angle of maximum angular density of the second branch of the PXR: $\theta_{\perp} \approx \sqrt{\gamma^{-2} - \chi'_0} \approx 10\text{mrad}$, which corresponds to Fig. 3. Fig. 3

shows the curves constructed using formula (17) describing the angular density of the second branch of the PXR. The curves in Fig. 2 and Fig. 3 are constructed for different values of the magnetic permeability of a single crystal μ and show a significant effect of the magnetic permeability of a single crystal on the spectral-angular and angular densities of parametric X-ray radiation. It should be noted that the angular densities of the PXR are symmetrical with respect to the ordinate axis. It follows from the figures that a small change in the magnetic permeability of a single crystal plate leads to a significant increase in the spectral-angular and angular densities of the PXR. This new interesting result is related to the fact that the resonance condition (14) becomes closer to zero in this case. In this case, the spectral-angular density of the PXR shifts according to expression (15). In the case of equality of the magnetic permeability of the unit in Fig. 2, the curve of the spectral-angular density of the PXR is not given, since it is small and is located significantly to the right of the given curves. It should also be noted that in the case when the single-crystal plate is tungsten, then for accurate calculations it is necessary to take into account its magnetic permeability: $\mu_w = 1.000068$.

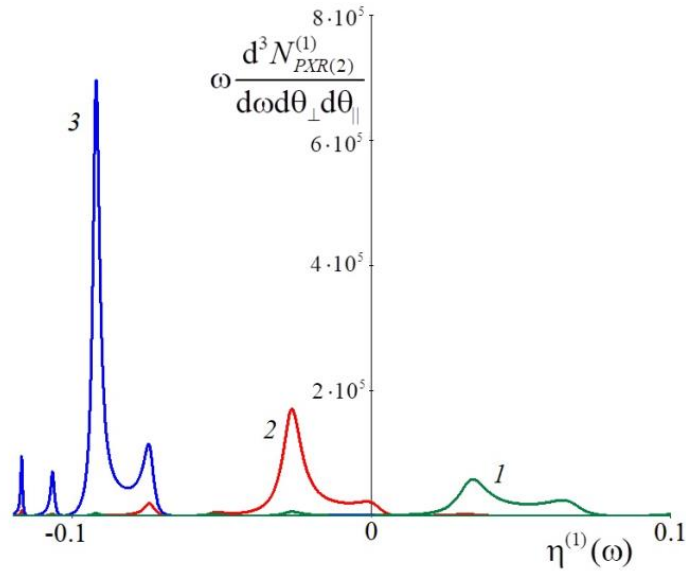


Fig.2 – Spectral-angular density of the second branch of the PXR for different magnetic permeabilities of a single crystal. Designations: 1 – $\mu = 1.00005$, 2 – $\mu_w = 1.000068$, 3 – $\mu = 1.00009$.

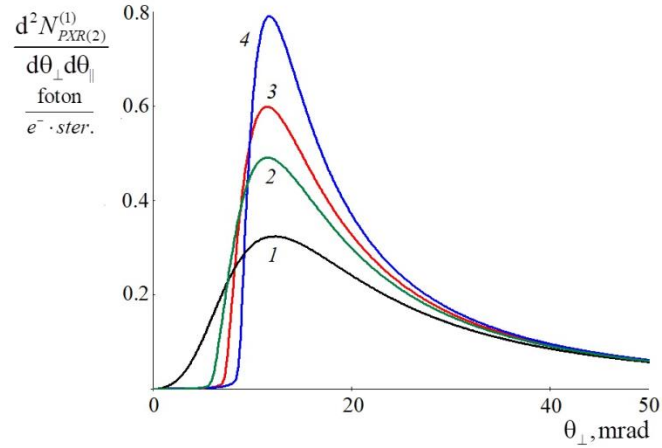


Fig.3 – Angular density of the second branch of the PXR for different magnetic permeabilities of a single crystal. Designations: 1– $\mu = 1$, 2– $\mu = 1.00005$, 3– $\mu_w = 1.000068$, 4– $\mu = 1.00009$.

Fig. 4 shows the curves constructed using formula (11), describing the spectral-angular densities of the first branch of the PXR, which correspond to the fulfillment of the resonance condition (13). The curves are constructed for the observation angle: $\theta_{\perp} = 4 \text{ mrad}$, $\theta_{\parallel} = 0$, which corresponds to the maximum angular density of the PXR. Fig. 5 shows the curves constructed using formula (17), describing the angular density of the first branch of the PXR. From the figures it follows that the first branch of the PXR depends significantly on the magnetic permeability of the single crystal under the conditions under consideration.

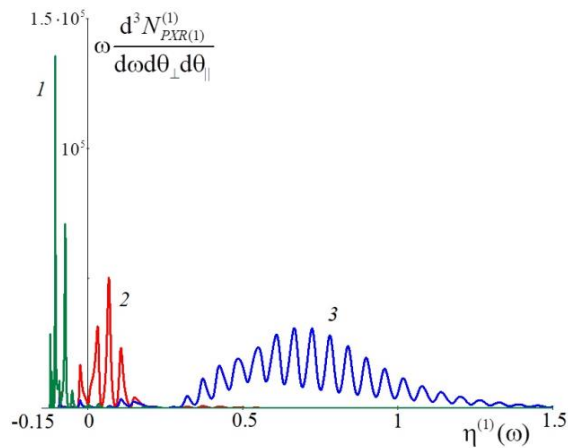


Fig.4 – Spectral-angular density of the first branch of the PXR for different magnetic permeabilities of a single crystal. Designations: 1– $\mu=1.00005$, 2– $\mu=1.000068$, 3 – $\mu=1.00009$.

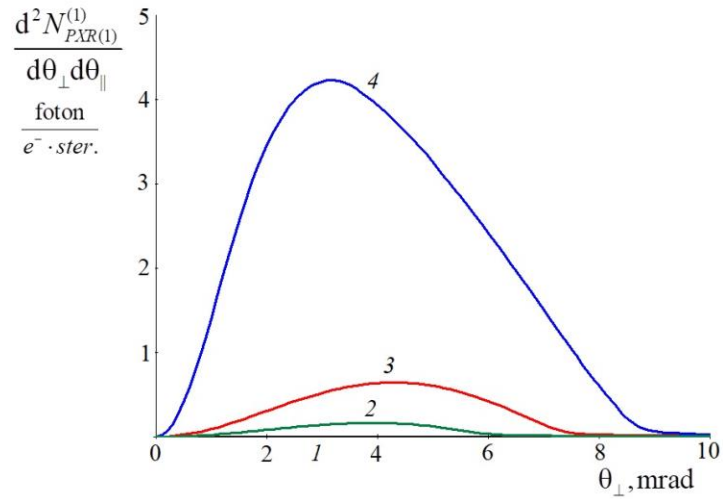


Fig.5 – Angular density of the second branch of the PXR for different magnetic permeabilities of a single crystal. Designations: 1– $\mu=1$, 2– $\mu=1.00005$, 3– $\mu=1.000068$, 4 – $\mu=1.00009$.

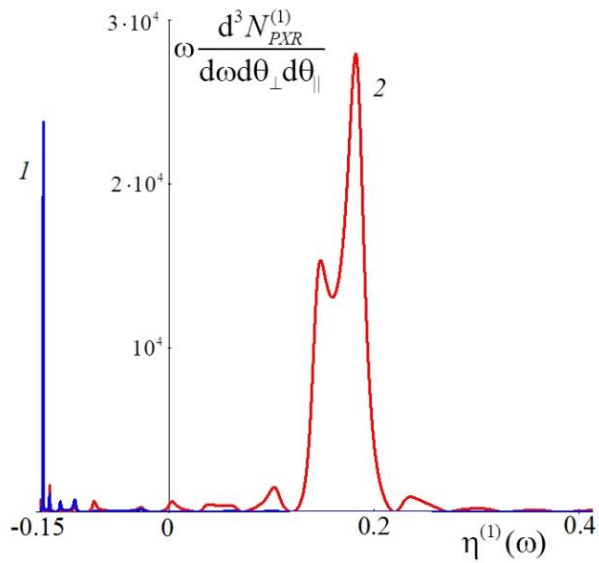


Fig.6 – Comparison of spectral-angular densities of the first and second branches of the PXR for magnetic permeability $\mu=1.00002$. Designations: 1 – the first branch of the PXR, observation angle $\theta_{\perp}=4\text{mrad}$, $\theta_{\parallel}=0$; 2 – the second branch of the PXR, observation angle $\theta_{\perp}=10\text{mrad}$, $\theta_{\parallel}=0$.

It should be noted that for magnetic permeability values close to unity, the first branch of the PXR has a negligibly small spectrum width compared to the second branch of the PXR, this is demonstrated by the curves shown in Fig. 6. This is due to the fact that the resonance condition of the first branch of the PXR (13) changes very quickly with a change in the frequency function $\eta^{(1)}(\omega)$ subject to the condition: $\sigma_*^{(s)} < \frac{1}{\sqrt{\epsilon}}$. When the magnetic permeability increases, the value $\sigma_*^{(s)}$ decreases, which leads to the fact that the resonance condition (13) changes more slowly with a change $\eta^{(1)}(\omega)$, while the spectrum width of the first branch of the PXR increases (Fig.4). This leads to a significant increase in the angular density of the first branch of the PXR (Fig.5).

From a comparison of Fig. 3 and Fig. 5 it follows that the angular densities of the first and second branches of the PXR exist simultaneously at different observation angles. In this case, the maximum of the angular density of the second branch of the PXR is located at an observation angle $\theta_{\perp} \approx \sqrt{\gamma^{-2} - \chi'_0}$, which corresponds to the usually accepted angle of maximum for the PXR. The maximum of the first branch of the PXR is at smaller observation angles. This is due to the fact that at these observation angles the resonance condition (13) for the first branch of the PXR is satisfied.

With an increase in the magnetic permeability of the single crystal, peaks appear in the angular density of the second branch of the PXR at small observation angles θ_{\perp} , which is demonstrated by the curves shown in Fig. 7 and Fig. 8. The appearance of such peaks is due to the fact that in the angular part of the angular density of the PXR (17), under the condition that the magnetic permeability is greater than one $\mu > 1$, the denominator can be equal to zero:

$$\gamma^{-2} + \theta_{\perp}^2 - \chi'_0 - 2(1 - 1/\sqrt{\mu}) = 0. \quad (21)$$

In this case, we obtain two points of maximum angular density:

$$\theta_{\perp} = \pm \sqrt{2(1 - 1/\sqrt{\mu}) + \chi'_0 - \gamma^{-2}}, \quad (22)$$

which determine the peaks in the angular density of the PXR in Fig. 7 and Fig. 8.

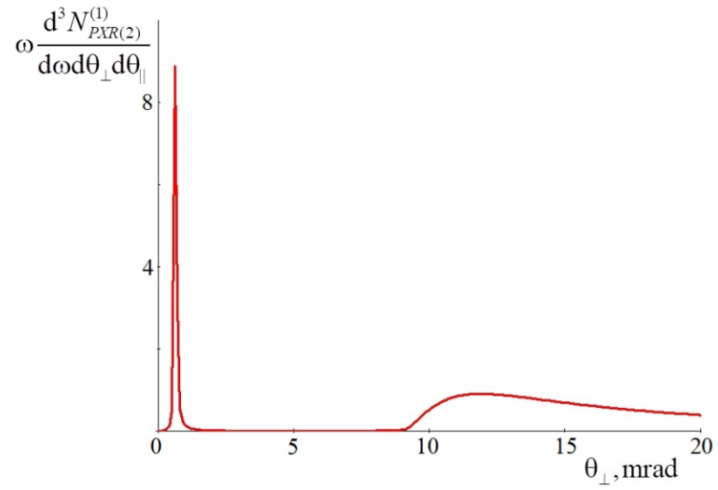


Fig.7 – Angular density of the second branch of the PXR for magnetic permeability $\mu = 1.0001$.

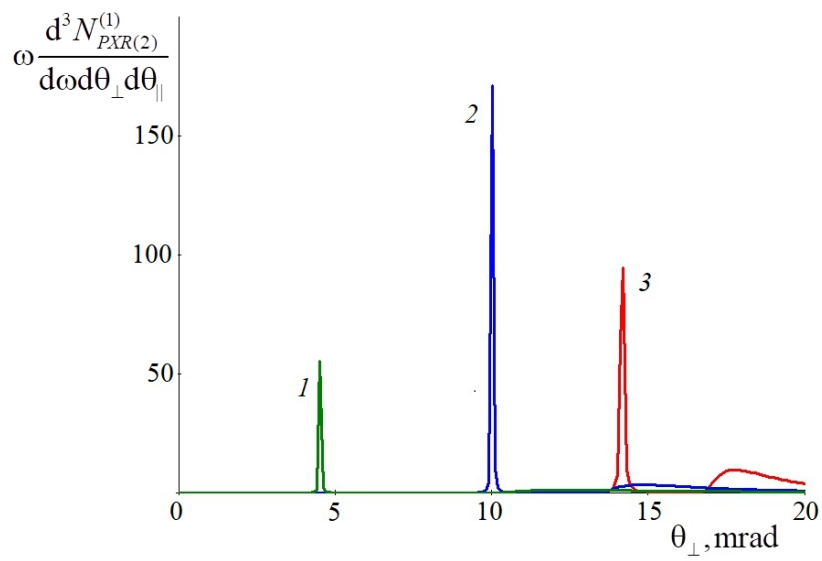


Fig.8 – Same as in Fig. 7, but for larger values of magnetic permeability. Designations: 1– $\mu = 1.00012$, 2– $\mu = 1.0002$, 3– $\mu = 1.0003$.

Since in the X-ray frequency range far from the region of anomalous dispersion, the real part of the average dielectric susceptibility is negative: $\chi'_0 < 0$, then in the case when $\mu=1$, equation (21) cannot have a real solution and expression (22) is complex. Obviously, the anomalous peaks in the angular density of PXR are manifestations of an effect similar to Vavilov-Cherenkov radiation, only in the X-ray frequency range of radiation. Indeed, in the case of $\mu=1$, solution (22) will correspond to the maximum of Vavilov-Cherenkov radiation at $\chi'_0 > 0$: $\theta_{\perp} = \pm\sqrt{\chi'_0 - \gamma^{-2}}$. In the X-ray frequency range of radiation, the condition: $\chi'_0 > 0$ is possible only in the region of anomalous dispersion, when the radiation frequencies are close to the frequencies of atomic radiation due to electron transitions in the atom. Thus, in the present work it was revealed that under certain conditions, by changing the magnetic permeability of a single-crystal plate, it is possible to obtain conditions for the generation of parametric X-ray radiation peaks, which have the nature of Vavilov-Cherenkov radiation.

In a real experiment, a single-crystal target is crossed by a beam of relativistic electrons, and the contribution of each electron to the spectral-angular and angular densities of the PXR is not coherent. The calculations were performed above for the case when one relativistic electron moves along the axis of the electron beam. In fact, the electron beam in a real experiment has an angular divergence of ψ_0 . Using the expressions (19) and (20) obtained in this paper, we will consider the effect of the electron beam divergence on the spectral-angular and angular densities of the PXR for different magnetic permeability's of the single-crystal plate.

Fig. 9 shows the curves constructed using formula (19) describing the spectral-angular density of the second branch of PXR at different angular divergence of the electron beam for magnetic permeability equal to unity $\mu=1$. The figure shows a decrease in the amplitude of the spectral-angular density of PXR and a slight increase in the width of the spectrum with an increase in the angular divergence of the electron beam. In the case when the angular divergence is equal to: $\psi_0 = 0.1\text{mrad}$, it has a very weak effect on the spectral-angular density under the conditions under consideration. Therefore, the curve for this divergence is not shown in the figure. The effect on the spectral-angular density of the divergence will be significant starting from $\psi_0 = 0.3\text{mrad}$, as shown in Fig. 9.

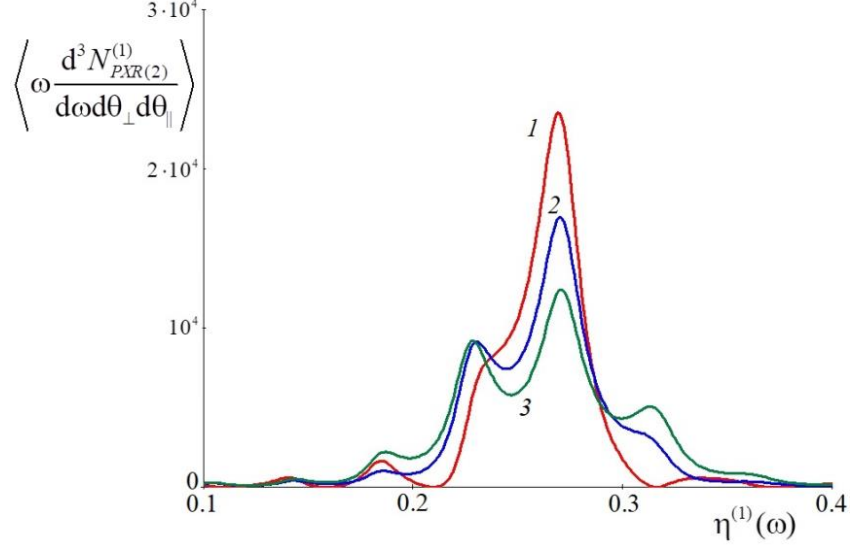


Fig.9 – Spectral-angular density of the second branch of PXR at different angular divergence of the electron beam. Magnetic permeability $\mu = 1$. Designations: 1– $\psi_0 = 0$, 2– $\psi_0 = 0.3$ mrad, 3– $\psi_0 = 0.5$ mrad.

Figure 10 shows curves similar to those in Figure 9, but with magnetic permeability equal to $\mu = 1.00009$. It follows from the figure that with an increase in the angular divergence of the electron beam, additional peaks in the spectral-angular density of the PXR appear and grow. This is due to the fact that with the magnetic permeability under consideration, the fulfillment of the resonance condition (14) significantly depends on the angle of deviation of the electron velocity $\psi(\psi_{\perp}, \psi_{\parallel})$ relative to the axis of the electron beam \mathbf{e}_1 . Therefore, when averaging the spectral-angular density of the PXR over various rectilinear trajectories of electrons in the beam, which are determined by the angle $\psi(\psi_{\perp}, \psi_{\parallel})$, additional spectral peaks of the PXR grow, while the amplitude of the main peak of the PXR decreases.

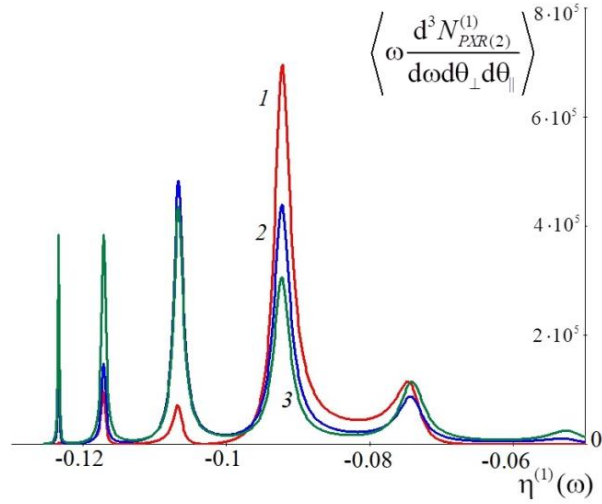


Fig.10 – Same as in Fig. 9, but with $\mu = 1.00009$. Designations: 1– $\psi_0 = 0$, 2– $\psi_0 = 0.3$ mrad, 3– $\psi_0 = 0.5$ mrad.

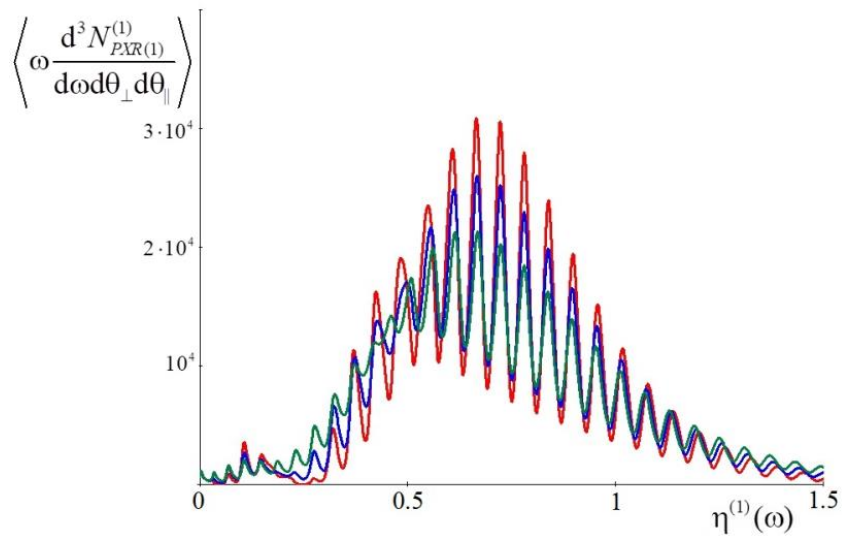


Fig.11 – Spectral-angular density of the first branch of PXR at different angular divergence of the electron beam. Magnetic permeability $\mu = 1.00009$. Designations: 1– $\psi_0 = 0$, 2– $\psi_0 = 0.3$ mrad, 3– $\psi_0 = 0.5$ mrad.

If the angular divergence of the electron beam is approximately equal to that characteristic of electron accelerators: $\psi_0 = 0.1 \text{ mrad}$, then the angular divergence will have no effect on the spectral-angular density under the conditions of the influence of the magnetic permeability of the single crystal on the spectral-angular density of the PXR. For the first branch of the PXR, the result is the same, this is demonstrated by the curves presented in Fig. 11

Let us consider the influence of the angular divergence of the electron beam on the angular density of the PXR. Fig. 12 and Fig. 13 show the curves constructed using formulas (20) describing the angular densities of the second and first branches of the PXR for different values of the angular divergence of the electron beam ψ_0 , for magnetic permeability equal to $\mu = 1.00009$. It follows from Fig. 12 that under the considered conditions, a significant dependence of the angular densities of the second and first branches of the PXR on the divergence of the electron beam begins with different values of the divergence angles $\psi_0 = 3 \text{ mrad}$ and $\psi_0 = 1 \text{ mrad}$, respectively. This is due to the fact that the angular density of the first branch of the PXR is at smaller observation angles than the angular density of the second branch of the PXR.

As a result, it can be noted that in a real experiment under the considered conditions, the angular divergence of the electron beam will not affect the angular density of the PXR. However, with a sufficiently large angular divergence of the electron beam, comparable to the value of the angle of the maximum of the PXR, the influence of the divergence will be significant, but will not affect the manifestation of effects associated with the influence of the magnetic permeability of the single crystal on the spectral-angular characteristics of the PXR.

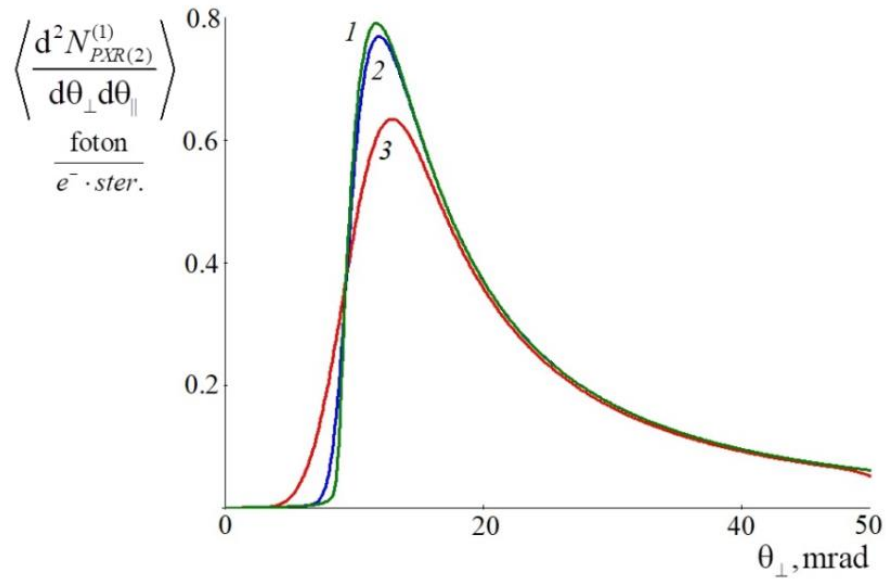


Fig.12 – Angular density of the second branch of PXR at different angular divergence of the electron beam. Magnetic permeability $\mu = 1.00009$. Designations: 1- $\psi_0 = 0$, 2- $\psi_0 = 1$ mrad, 3- $\psi_0 = 3$ mrad

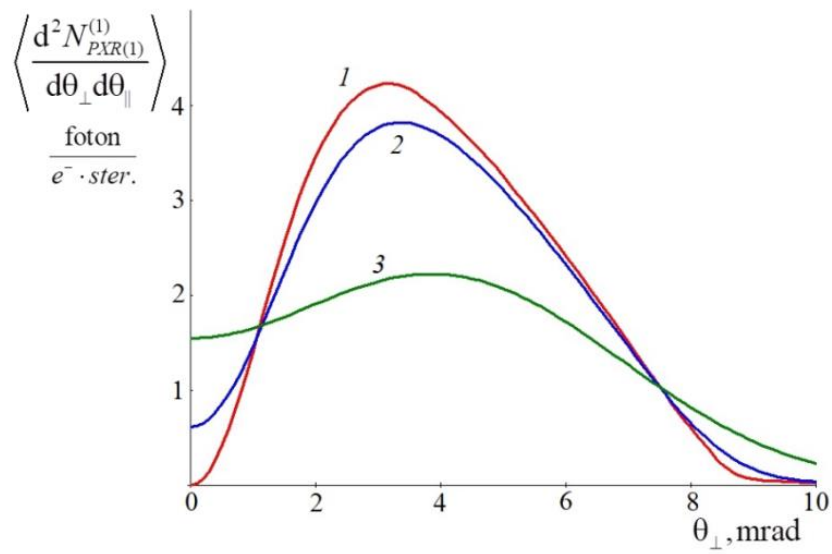


Fig.13 – Angular density of the first branch of PXR for different angular divergence of the electron beam. Magnetic permeability $\mu = 1.00009$. Designations: 1– $\psi_0 = 0$, 2– $\psi_0 = 1\text{mrad}$, 3– $\psi_0 = 3\text{mrad}$.

5. CONCLUSION

In the work, within the framework of the two-wave approximation of the dynamic theory of diffraction, a theory of parametric X-ray radiation of beams of relativistic electrons intersecting a magnetized single-crystal plate is developed. Expressions are obtained that describe the spectral-angular and angular densities of two branches of the PXR, including the magnetic permeability of the single crystal μ . It is shown that under the condition $\mu > 1$, both branches of the PXR can be significant simultaneously, but at different observation angles. A significant increase in the spectral-angular and angular densities of both branches of the PXR with an increase in the magnetic permeability of the single crystal in a certain range, which depends on the parameters of the radiation process, is shown.

It is shown that at certain values of μ , there are conditions when an effect similar to the Vavilov-Cherenkov effect can appear in the PXR. As a result of this effect, peaks appear in the angular density of the PXR, which were previously not observed or predicted by anyone. Expressions describing the spectral-angular and angular densities of two branches of the PXR taking into account the angular divergence of the relativistic electron beam are obtained. It is shown that the angular divergence of the electron beam in real experiments will not affect the manifestations of effects associated with the influence of the magnetic permeability of the single crystal on the spectral-angular characteristics of the PXR. At a sufficiently large angular divergence of the electron beam, comparable with the value of the angle of the maximum of the PXR, the influence of the electron beam divergence will be significant. It is shown that this will not affect the manifestations of effects associated with the influence of the magnetic permeability of the single crystal on the spectral-angular characteristics of the PXR.

REFERENCES

1. M.L. Ter-Mikaelian, *High-Energy Electromagnetic Processes in Condensed Media*, Wiley, New York, 1972.
2. G.M. Garibian, C. Yang, *J. Exp. Theor. Phys.* **61**, 930 (1971).
3. V.G. Baryshevsky, I.D. Feranchuk, *J. Exp. Theor. Phys.* **61**, 944 (1971).
4. H. Nitta, *Phys. Lett. A* **158**, 270 (1991).
5. I.D. Feranchuk, A.V. Ivashin, *J. Physique* **46**, 1981 (1985).
6. A.S. Kubankin, N.N. Nasonov, V.I. Sergienko, I.E. Vnukov, *Nucl. Instrum. Methods Phys. Res. B* **201**, 97 (2003).

7. N. Nasonov, A. Noskov, Nucl. Instrum. Methods Phys. Res. B. **201**, 67 (2003).
8. V.G. Baryshevsky I. D. Feranchuk A. P. Ulyanenko, *Parametric X-ray Radiation in Crystals: Theory, Experiments and Applications*, Springer (2005).
9. S.V. Blazhevich, A.V. Noskov, Nucl. Instrum. Methods Phys. Res. B. **266**, 3770 (2008).
10. S.V. Blazhevich, A.V. Noskov, Journal of Experimental and Theoretical Physics. **123**, 551 (2016).
11. S.V. Blazhevich, K.S. Lyushina, A.V. Noskov, Journal of Experimental and Theoretical Physics. **128**, 212 (2019).
12. S.R. Uglov, V.V. Kaplin, A.S. Kubankin et.al., Journal of Physics: Conference Series. **732**, 012017 (2016).
13. S.R. Uglov, V.V. Kaplin, A.S. Kubankin et.al., Journal of Physics: Conference Series. **732**, 012017 (2016).
14. S. Huang, R. Duan, N. Pramanik, J.S. Herrin, C. Boothroyd, Z. Liu & L.J. Wong, Nature Photonics. **17**, 24 (2023).
15. S. Huang, R. Duan, N. Pramanik, C. Boothroyd, Z. Liu, L.J. Wong, Advanced Science. **9** (16), 2105401 (2022).
16. A.V. Noskov, S.V. Blazhevich, Journal of Instrumentation. **19**, P07007 (2024).
17. A.V. Noskov, S.V. Blazhevich, Physics Letters A. **525**, P129835 (2024).
18. A.V. Noskov, S.V. Blazhevich, E.D. Pronina, Journal of Instrumentation. **20**, P06015 (2025).